# Communication

# A Small-Clearance High-Efficiency Dual-Band Wi-Fi 6E Antenna Taking Advantage of an All-Metal Laptop

Weihao Diao, Yue Li, Le Chang, Qiao Guan, and Zhijun Zhang

***Abstract*—A small-clearance dual-band Wi-Fi 6E antenna optimized for an all-metal industrial design (ID) laptop is proposed. The antenna features a $\pi$-shaped strip within the hinge-side open slot, effectively exciting side-edge ground currents to maximize radiation efficiency. This approach circumvents the limitations of traditional IFA or slot antennas, which require either complex cuts or protruding structures. Thus, it achieves seamless integration with all-metal covers without structural compromises. Leveraging the efficient ground current excitation, the antenna significantly expands the radiating aperture, achieving broadband and high-efficiency performance within an ultra-small clearance of 4.7 × 29.4 mm$^2$. Configured as a 2 × 2 MIMO system, the antenna achieves a −10 dB impedance bandwidth of 2.24–2.55 GHz (LB) and 4.94–7.5 GHz (HB), with efficiencies exceeding 79% (LB) and 66% (HB). The envelope correlation coefficient (ECC) remains below 0.03, ensuring excellent MIMO performance. The proposed antenna fully covers the Wi-Fi 6E bands (2.4G/5G/6G) while maintaining high isolation, wide bandwidth, and robust compatibility with all-metal ID laptops.**

***Index Terms*—All-metal industrial design (ID), dual-band, ground current, hinge, laptop antenna, small clearance area, wideband, Wi-Fi 6E.**

## I. Introduction

Wi-Fi 6E, spanning from 2.4 to 2.48 GHz, 5.15 to 5.85 GHz, and 5.925 to 7.125 GHz, offers expanded spectrum, higher bandwidth, and lower latency. This development is significant for modern laptops, where the demand for faster, more reliable wireless connections is ever-growing. As laptops continue to integrate more components and adopt narrow-bezel, all-metal enclosures, the laptop antennas face new challenges, particularly in achieving small sizes, small clearance areas, and broad bandwidth while maintaining high performance.

Chu's limit constrains antenna bandwidth by size, thus slim-bezel all-metal laptop antennas' minimal clearance challenging wide bandwidth and high efficiency realization.

Various approaches have been explored to enhance bandwidth in laptop antennas, such as coupling feed [1], [2] multi branches [3], [4], p-i-n diode for reconfiguration [5], bowtie feed [6], slot loading [7], and multi modes [8], [9], [10] and so on. For miniaturization, methods such as grooving [9], PCB double-sided printing [12], curving and folding [13], [14] can be used. The approaches above basically place an IFA or monopole at the top of the screen. While capable of achieving wide bandwidth, they are incompatible with narrow-bezel full-metal laptops due to the restricted bezel width, the metal cover shielding, and limitations on visible metallic modifications.

In tablet designs, the metal frame and ground plane can be cut into loops [15], [17], slots [17], [18], or hybrid configurations [19], [20], enabling wide band with small clearance. However, all-metal laptops usually prohibit visible complex cuts on metal covers to maintain the structural integrity, limiting the implication of these methods.

Several strategies have been proposed to tackle the antenna design for all-metal industrial design (ID) laptops. For instance, a hybrid loop/monopole antenna with a back cavity was proposed in [21]. While this achieves compatibility with small clearance, it increases total volume. A patch antenna with parasitic monopoles on a high-permittivity ceramic substrate was proposed in [22], but this often leads to narrow bandwidth and low efficiency. Other approaches use the central hinge slot to achieve wide bandwidths [23], [24], [25]. Multi-branch feeder [23], coupling feed [24], and additional slots [25] can be utilized to excite multiple modes of hinge slot. However, using the hinge slot as a resonator may increase the clearance area. Moreover, the broadband excitation of the slot may compromise the structural integrity of the metal enclosure, leading to issues of compatibility and reliability.

This communication proposes a small-clearance dual-band Wi-Fi 6E antenna that leverages the metal covers of an all-metal laptop. The proposed antenna is a folded $\pi$-shaped strip placed within the hinge side slot, whose clearance area is as small as 4.7 × 29.4 mm. The traveling wave currents are effectively excited on the metal cover by the strip. Thus, the effective radiating aperture is largely extended, contributing to a high efficiency and broad bandwidth. The 2 × 2 MIMO antenna system composed of two proposed antennas at the two outside slots next to the hinges exhibits a −10 dB IBW of 2.24–2.55 GHz (12.9%) in the LB, and 4.94–7.5 GHz (41.5%) in the HB, with efficiencies exceeding 79% and 66%, respectively, an isolation higher than 33 dB and an envelope correlation coefficient (ECC) below 0.03.

The main contributions of this study are as follows.

1) Excites side-edge ground-plane currents using a folded $\pi$-shaped strip within the hinge-side slot, achieving compatibility with narrow-bezel full-metal laptops.
2) Achieves ultra-compact clearance, broadband performance, and high efficiency, with a radiation aperture far exceeding the clearance area by exciting the side-edge ground current.
3) Provides inherent high isolation for a 2 × 2 MIMO system through the physical separation and independent excitation of ground-plane currents on opposite edges.

## II. Antenna Configuration

Fig. 1 shows the configuration of the proposed antenna. In the all-metal ID, the screen plate and keyboard plate can be simplified as two single-sided copper-clad FR4 boards, as depicted in Fig. 1(a). The hinges in the laptop are marked with black dashed elliptical frames. The proposed antennas are situated in the outer slots near the hinges, indicated by red boxes. The left and right antennas are identical, designed for MIMO applications.

Received 17 December 2024; revised 17 March 2025; accepted 9 April 2025. Date of publication 25 April 2025; date of current version 6 August 2025. This work was supported by the National Natural Science Foundation of China under Contract 62271279. *(Corresponding author: Zhijun Zhang.)*

Weihao Diao, Yue Li, and Zhijun Zhang are with the Department of Electronic Engineering and Beijing National Research Center for Information Science and Technology (BNRist), Tsinghua University, Beijing 100084, China (e-mail: zjzh@tsinghua.edu.cn).

Le Chang is with the School of Information and Communications Engineering, Xi'an Jiaotong University, Xi'an 710049, China (e-mail: changle@xjtu.edu.cn).

Qiao Guan is with Honor Device Company Ltd., Xian 710100, China (e-mail: guanqiao@honor.com).

Digital Object Identifier 10.1109/TAP.2025.3562775

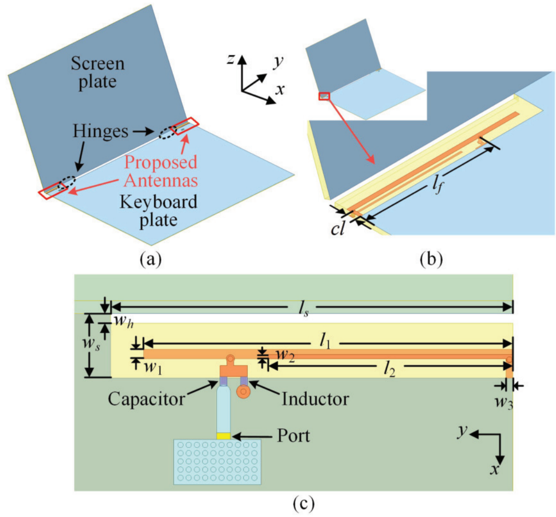


Fig. 1. Configuration of the proposed antenna: (a) antenna's position in a laptop, (b) enlarged perspective view, and (c) bottom view of the antenna.

TABLE I

DETAILED DIMENSIONS OF THE PROPOSED ANTENNA

| $l_s$ | $l_1$ | $l_2$ | $l_f$ | $cl$ | $w_1$ | $w_2$ | $w_3$ | $w_h$ | $w_s$ |
|---|---|---|---|---|---|---|---|---|---|
| 29.4 | 28 | 17.9 | 20.6 | 1.4 | 0.7 | 0.3 | 0.5 | 0.7 | 4.7 |

The unit of all parameters is mm.

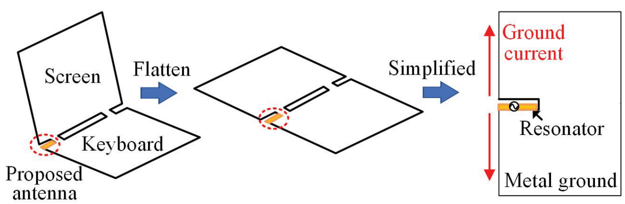


Fig. 2. Simplification in the analysis of the proposed antenna and working principle of the proposed antenna.

Enlarged views of the proposed antenna are illustrated in Fig. 1(b) and (c). The antenna is in a folded $\pi$-shaped strip form printed on both sides of an FR4 substrate with a relative permittivity of 4.7 and a loss tangent of 0.02. A shunt inductance (muRata LQW04AN5N6) of 5.6 nH and a series capacitor (FENGHUA 0402RF0R8C) of 0.8 pF are utilized for LB matching. In Fig. 1, the folded $\pi$-shaped strip and the ground are in different colors to emphasize the location and structure of the proposed antenna. The two parallel sections of the strip along the slot are connected by a metallized via at the edge of the substrate. The shorting point is aligned with the slot opening.

The clearance area of the antenna in an all-metal ID laptop is defined as the space cut out for the antenna, including the area occupied by the antenna itself. Thus, the outer slot, with a minimal size of $4.7 \times 29.4$ mm$^2$, represents the clearance area of the proposed antenna. The detailed dimensions of the proposed antenna are provided in Table I. The overall size of both the screen plate and keyboard plate (1-mm-thick single-sided copper-clad FR4 boards) is $304 \times 227$ mm$^2$. The hinge slot in the middle has a length of 185.2 mm, and the hinges themselves are 30 mm long.

## III. ANTENNA ANALYSIS AND WORKING MECHANISM

First, a single proposed antenna will be analyzed. To facilitate the analysis, some simplification is needed. The simplification and the working principle of the proposed antenna are demonstrated in Fig. 2. In the simplification, the two plates are unfolded to 180°, and the middle long slot and another side slot are removed. As shown, the folded $\pi$-shaped strip serves as a resonator within the open slot to excite the ground current to radiate. The effective radiation aperture is remarkably enlarged while the clearance area is only the area of the side slot. Hence, the proposed antenna can realize a high efficiency and a wide bandwidth while maintaining a small clearance area.

It should be noted that the resonant modes of the folded $\pi$-shaped strip will not be affected in most of the angle between the two plates, which will be shown later. The plates are the ground and there is no resonance on the ground. Besides, the long slot between the two hinges has no effect on the proposed antenna because the excited current primarily flows on the ground edge, which will be shown later. Thereby, the analysis on the proposed antenna is based on the simplified model in this section.

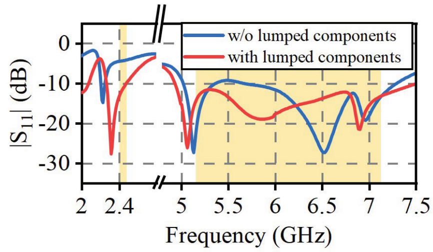


Fig. 3. Reflection coefficients of the proposed antenna with or without the lumped components.

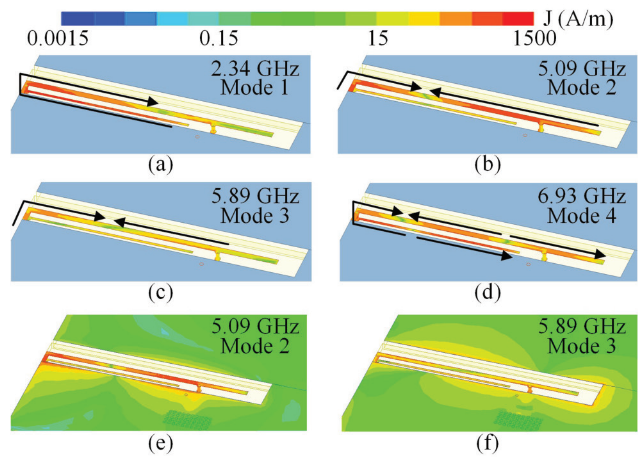


Fig. 4. Current distribution at different resonances on the folded $\pi$-shaped strip: (a) 2.34, (b) 5.09, (c) 5.89, and (d) 6.93 (unit: GHz). Current distributions on the strip and the ground in (e) 5.09 and (d) 5.89 GHz.

### A. Resonant Modes of the Folded $\pi$-Shaped Strip

The reflection coefficients of the proposed antenna with or without the lumped components are depicted in Fig. 3. The bands of Wi-Fi 6E are highlighted in yellow. As shown, the LB matching improved the lumped components, and the IBW of the LB is 2.26–2.5 GHz (10.1%). Note that the wide bandwidth is primarily due to the excitation of ground plane currents, which inherently provides the broadband characteristic. The lumped components only serve to improve impedance matching to 50 Ω within this frequency band. This will be discussed in detail in Section III-B.

The resonance covering the LB is at 2.34 GHz, while in the HB, there are three resonances at 5.09, 5.89, and 6.93 GHz. These resonances are generated by the folded $\pi$-shaped strip. The current distributions on the strip at different resonances are shown in Fig. 4.

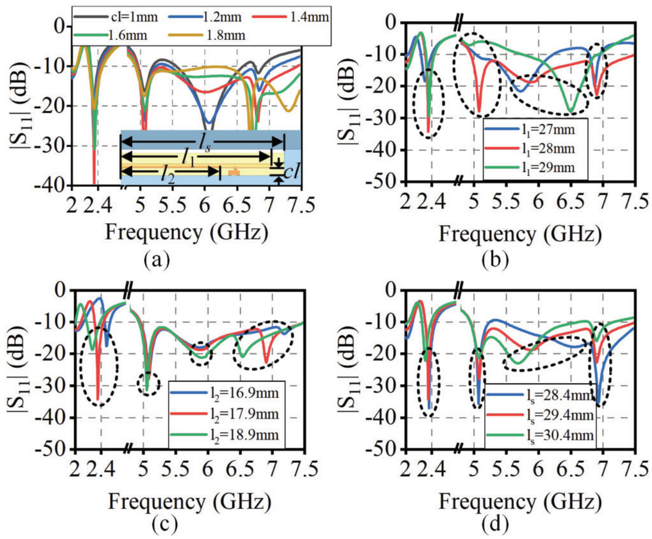


Fig. 5. Reflection coefficients in the parameters study of the proposed antenna: (a) $cl$, (b) $l_1$, (c) $l_2$, and (d) $l_s$.

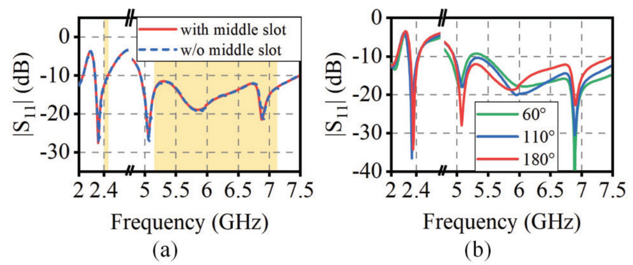


Fig. 6. Reflection coefficients of the proposed antenna (a) with or without the middle long slot and (b) with different angles between the two plates.

The direction of the current is marked with black arrows in Fig. 4. It can be seen that the resonances are respectively the $\lambda/2$ mode of the strip (mode 1), the third mode of the IFA (mode 2), a hybrid mode (mode 3), and the $2\lambda$ mode of the strip (mode 4) from Fig. 4(a) to (d). Though the current distributions on the strip are similar in modes 2 and 3, the resonances are different. Fig. 4(d) and (e) displays the current distributions on the strip and the ground in the two modes. It can be seen there is strong image current on the slot edge closer to the strip in mode 2, confirming that mode 2 is the third mode of the IFA. In mode 3, the current distributes on both edges of the slot owing to the energy coupled from the strip to the slot.

For a clearer perspective of the modes, the reflection coefficients of the proposed antenna with different sizes of the folded $\pi$-shaped strip are plotted in Fig. 5. The downright inset of Fig. 5(a) labeled the studied parameters. As seen, the reflection coefficient is insensitive to the variation of the distance $cl$ between the strip. Each black dashed ellipse outlined in Fig. 5 represents the same mode with different parameter values. As seen, the frequency of Mode 1 is only affected by $l_2$ because its resonant current primarily concentrates on the shorter branch and its facing part, as shown in Fig. 4(a). Mode 2 is only impacted by $l_1$ because its resonant current mainly concentrates on the longer branch, as shown in Fig. 4(b). $l_1$ and $l_s$ affect the frequency of Mode 3 on account of the coupling between the strip and the slot in Mode 3. The frequency of Mode 4 is hardly influenced by $l_1$ because the part of the strip's longer branch near the feeding point is not totally resonate with the other parts.

In the analysis above, the middle slot is removed and the angle between the two plates is set as 180° for simplicity. Actually, because the resonances are generated by the folded $\pi$-shaped strip, the modes

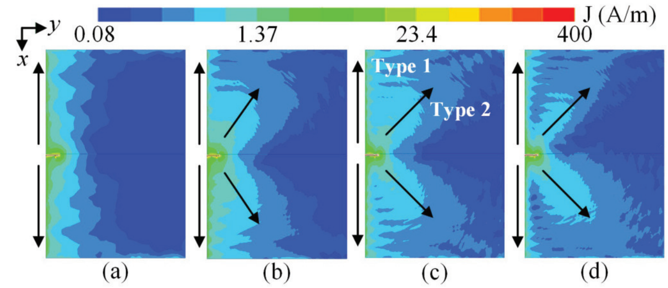


Fig. 7. Complex magnitude of current distributions on the ground at different frequencies: (a) 2.34, (b) 5.09, (c) 5.89, and (d) 6.93 (unit: GHz).

are scarcely affected by the middle slot and the angle. The reflection coefficients of the proposed antenna with or without the middle long slot are plotted in Fig. 6(a), and that with different angles between the two plates are shown in Fig. 6(b). As seen, the reflection coefficient is hardly affected by the middle slot and the angle.

### B. Utili z Ation of the Metal Covers

The metal enclosures of the all-metal ID laptop serve as the ground. The proposed antenna takes advantage of the metal covers by exciting the traveling wave current on them, which can be called the ground current. The current distributions on the metal cover (or ground) at different frequencies are illustrated in Fig. 7. There are two types of current: type 1 flowing along the ground edge ($\pm x$-directions) while type 2 flowing toward upper right and lower right directions on the ground plane. Type 1 is the traveling wave current excited on the ground, which radiates during its propagation, and type 2 is the current induced by the radiation field of the slot. In the LB, there is only type 1 because the aperture of the slot is too small to radiate well. Hence, the LB primary radiation is contributed by the ground current, leading to wide IBW and high efficiency. In the HB, the aperture of the slot is large enough to radiate part of the energy, leading to the induction of type 2 current on the ground plane. Additionally, the current radiates at the opening of the slot in the HB because the aperture of the slot opening is also large enough. The electromagnetic wave propagating through the slot will radiate when it reaches the discontinuity formed by the opening, resembling a Vivaldi antenna [26]. It can be noticed in Fig. 7(b) that type 1 current propagating in $+x$-direction is stronger than that in $-x$-direction due to the imbalanced IFA mode of the strip.

The radiation patterns of the proposed antenna at different modes are shown in Fig. 8 with the posture of the laptop model in the upper left. The proposed antenna radiates three types of beams, as marked in black dashed frame and labeled by numbers. Beam 1 is the radiation of the traveling wave current on the ground edge. Because the current flows at the left edge of the big metal ground, there is a defect on the right of the conical beam. Beam 2 is the wide beam radiated by the slot opening. At the HB, the currents radiate as they transition from the slot edge to the ground edge, similar to a Vivaldi antenna. The right-angle opening results in a broad beam. Beam 3 is the radiation of the slot, and it is nearly symmetric about the $xoy$ plane and the $xoz$ plane. The high ripples on the beams are mainly caused by the edge diffraction of the big ground. It can be seen in Fig. 8(a) that beam 1 is the dominant beam of the radiation pattern in the LB, proving the excitation of the traveling wave current on the ground. Thus, the effective aperture in the LB is far larger than the clearance area, contributing to a wide IBW and a high efficiency. In the HB, the aperture of the slot and the slot's opening are large enough, so beams 2 and 3 are generated. At 5.09 GHz, the primary beams are beams 1 and 3. Since in mode 2, the traveling wave current propagating in $+x$-direction is significantly stronger than that propagating in $-x$-direction, as shown in Fig. 7(b), the gain of the defected conical beam in the $-x$-direction is higher, while there is almost no beam 1 in

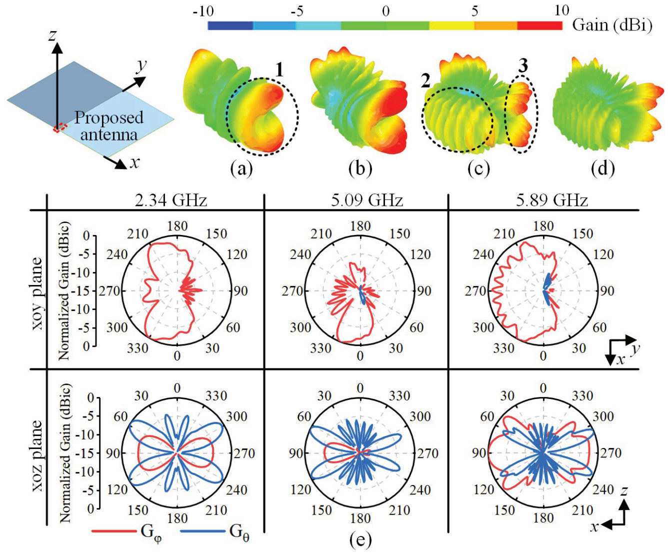


Fig. 8. 3-D Radiation patterns of the proposed antenna at different frequencies: (a) 2.34, (b) 5.09, (c) 5.89, (d) 6.93 (unit: GHz). (e) Normalized radiation patterns of the proposed antenna in different planes and frequencies.

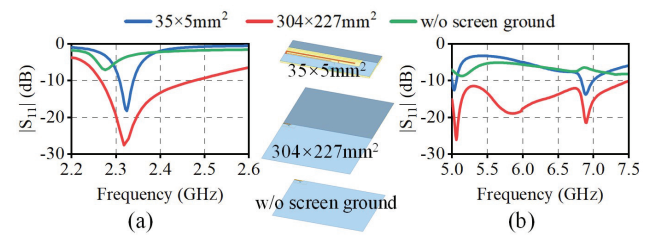


Fig. 9. Reflection coefficients of the proposed antenna in large, small ground and without the screen ground in (a) LB and (b) HB.

the $+x$-direction. This unbalanced current distribution also explains why beam 2 is hardly visible at 5.09 GHz. At 5.89 and 6.83 GHz, the primary beams are beams 2 and 3, with beam 1 almost absent, because the currents on the ground plane at these frequencies are more balanced, as shown in Fig. 7(b) and (c). These currents radiate directly toward the slot opening ($-y$-direction) as they pass through the slot like a Vivaldi antenna does. The radiation patterns in the *xoy* plane and the *xoz* plane are shown in Fig. 8(e). The patterns at 6.93 GHz are omitted due to their similarity to that at 5.89 GHz. In the *xoy* plane, the co-polarization is $\varphi$-polarization, which is polarization of the traveling wave current on the ground edge and the slot opening. In the *xoz* plane, $\theta$-polarization is the radiation of the ground current along the $\pm x$-directions, and $\varphi$-polarization in the HB is the radiation of the slot opening and slot itself. Besides, the ground current will turn to $y$-direction when it meets the corner, thus contributing to $\varphi$-polarization in the LB. In Fig. 8(e) the defected conical beam (beam 1) and the wide beam with ripple (beam 2) can be observed more clearly.

The reflection coefficients of the proposed antenna in different ground sizes and without the screen ground are plotted in Fig. 9. The values of the lumped components are adjusted to ensure the match of the LB. Despite the matching being optimized by lumped components, when the ground plane size is reduced from $304 \times 227$ mm$^2$ to $35 \times 5$ mm$^2$, the low-frequency matching bandwidth decreases from 2.26– 2.5 GHz (10.1%) to 2.31–2.34 GHz (1.3%). This clearly demonstrates that the wide bandwidth at low frequencies is due to the excitation of traveling wave currents on the ground plane. When the ground plane is reduced to a very small size, no traveling wave currents are present, resulting in a drastic narrowing of the bandwidth. For higher frequencies, the resonance still exists after reducing the

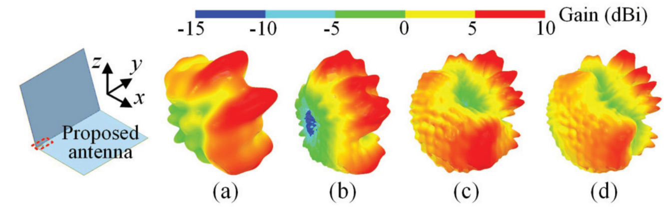


Fig. 10. Radiation patterns of the proposed antenna at different frequencies when the laptop model opens at the angle of 110°: (a) 2.34, (b) 5.09, (c) 5.89, (d) 6.93 (unit: GHz).

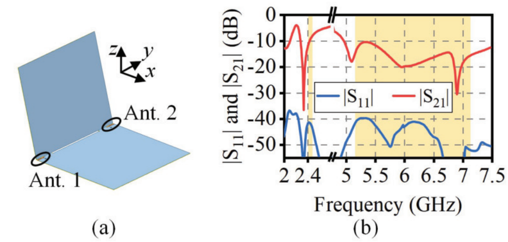


Fig. 11. (a) Configuration and (b) S parameters of the $2 \times 2$ MIMO antenna system.

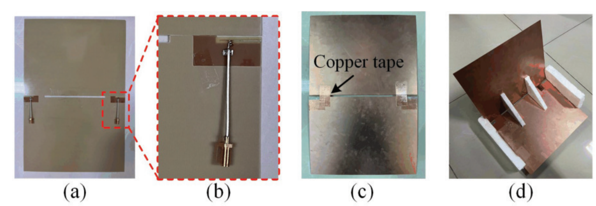


Fig. 12. Photograph of the proposed antenna on a simplified laptop model: (a) dielectric side, (b) metal side, (c) enlarged view of the proposed antenna, and (d) laptop model in 110°.

ground plane size, but the matching deteriorates. This is because the smaller ground plane leads to a reduced aperture. Besides, it can be seen in Fig. 9 that when the screen ground is absent, the reflection coefficient deteriorates dramatically in both bands. The analysis above indicates the excitation of the ground side-edge current contributes to the excellent performance of the proposed antenna.

Because of the excitation of the ground current, the angle between the two plates will affect the radiation patterns of the proposed antenna. The radiation patterns when the laptop model opens at the angle of 110° are demonstrated in Fig. 10. The two plates form a horn-like structure, guiding energy radiated from the slot to the angle flaring. Thus, the gain of the lobes of beam 3 pointing to the angle flaring will become higher. Moreover, the change of the angle also leads to the change of the beam direction of beam 1 and the deformation of beam 2.

### *C. 2 × 2 MIMO Antenna System*

By placing the proposed antennas into the two side slots, the $2 \times 2$ MIMO antenna system can be constructed, as shown in Fig. 11(a). The angle between the two plates is set as the usage angle of 110° and it has little effect on the S parameters as is analyzed in Section III-A. The S parameters of the MIMO system are plotted in Fig. 11(b). $|S_{22}|$ is omitted because it overlaps $|S_{11}|$. It can be observed that the working band of the proposed antenna covers all bands of Wi-Fi 6E. The mutual coupling is remarkably low owing to the long distance between the two antennas.

## IV. Experimental Verification

A prototype of the proposed antennas on a simplified laptop model was fabricated as shown in Fig. 12. The substrates of the folded

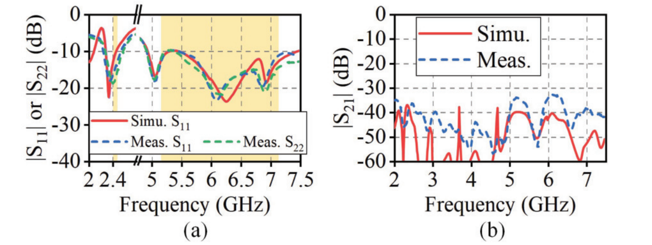


Fig. 13. Simulated and measured S parameters of the proposed antenna. (a) $|S_{11}|$ and $|S_{22}|$. (b) $|S_{21}|$.

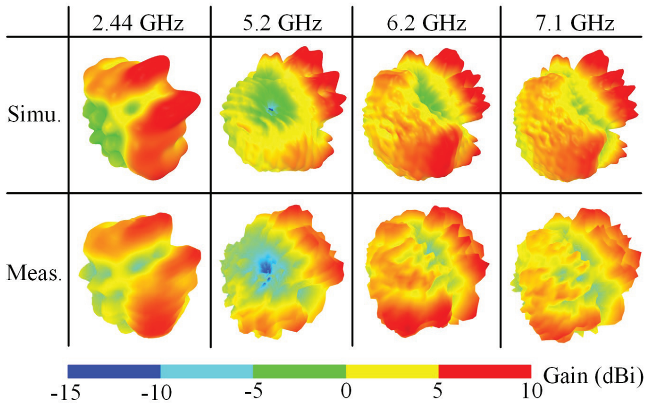


Fig. 14. 3-D radiation patterns of the proposed $2 \times 2$ MIMO antenna system.

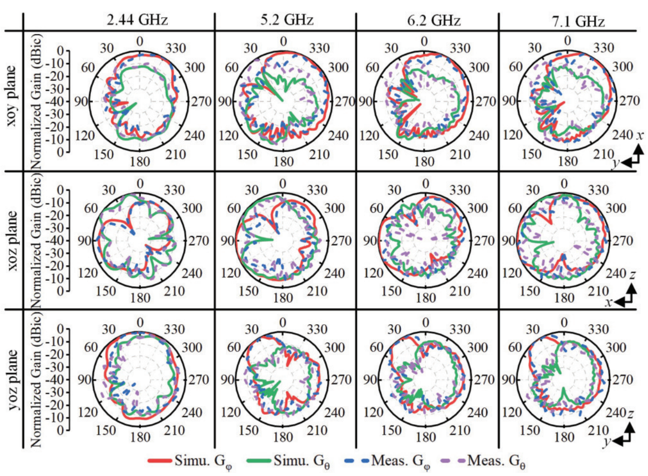


Fig. 15. 2-D normalized radiation patterns of the proposed $2 \times 2$ MIMO antenna system at different planes and different frequencies.

$\pi$-shaped strips are co-grounded with the two plates by copper taps, and coaxial cables are used for test. Fig. 12(b) displays the enlarged view of the proposed antenna. The laptop model in the angle of 110° for measurement is shown in Fig. 12(d).

The measured and simulated S parameters are plotted in Fig. 13. Only simulated $|S_{11}|$ is displayed in Fig. 13(a), because the simulated $|S_{11}|$ and $|S_{22}|$ overlap each other. As shown, the simulated −10 dB IBW of the proposed antenna is 2.26–2.5 GHz in the LB, and 4.94–7.5 GHz in the HB. The measured −10 dB IBW is 2.24–2.55 GHz in the LB, and 4.92–7.5 GHz in the HB. In the entire band, the mutual coupling of the two antennas is lower than −33 dB, as shown in Fig. 13(b). Hence, all bands of Wi-Fi 6E (2.4G/5G/6G) are well covered.

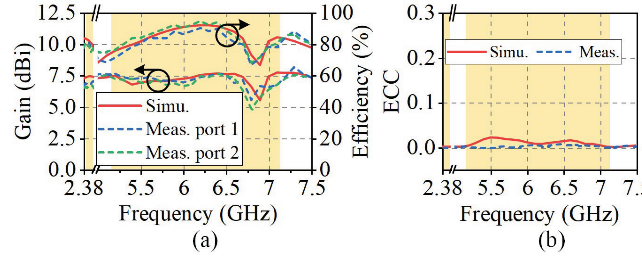


Fig. 16. Simulated and measured gain, efficiency, and ECC of the proposed antenna: (a) gain and efficiency and (b) ECC.

The 3-D simulated and measured radiation patterns of the proposed antenna at different frequencies in Wi-Fi 6E bands are illustrated in Fig. 14. On account of the symmetry between antenna 1 and 2, only the radiation patterns of antenna 1 are shown. The corresponding posture of the laptop model is the same as that shown in Fig. 11(a). Because 5.2 GHz is close to the frequency of mode 2 (5.09 GHz), the gain of the wide beam (beam 2) is lower. Despite this, the shape of radiation patterns in the HB is stable in the HB of Wi-Fi 6E. Because the HB of Wi-Fi 6E band is mainly covered by modes 3 and 4, the beam types of the radiation patterns are primarily beams 2 and 3, as is analyzed in Section III. The radiation in the HB counts on the slot opening and the slot. The 2-D radiation patterns of antenna 1 in the proposed MIMO system at different planes and different frequencies are shown in Fig. 15. Note that cross polarization is generally not an important factor of a laptop antenna. A laptop is typically used indoors where electromagnetic waves undergo multiple reflections and refractions. As a result, the polarization of the waves often changes after several reflections and refractions. The simulated radiation patterns coincide with those of measurement. The difference between the simulation and the measurement is attributed to the fabrication tolerance and the error of manual assembly.

The simulated and measured gain, efficiency, and ECC of the proposed antenna are plotted in Fig. 16. It can be seen that there is a pit on the efficiency curve at 6.9 GHz, the resonant frequency of Mode 4. As analyzed in Section III, the currents on the strip's folding parts facing each other are out of phase, so there is strong field concentrating between the two parts. Thus, the dielectric loss of the $2\lambda$ mode is high, decreasing the efficiency. However, it is acceptable because the lowest efficiency is still over 66%. The reason for the pit of the gain is the same. Notably, the efficiency of the LB exceeds 79%, which is remarkably high, because the radiator in the LB is the traveling ground current. The efficiency of the proposed antenna is over 79% at the lower frequencies and over 66% at higher frequencies in Wi-Fi 6E bands. To improve the HB efficiency, the parameters can be modified to shift the high loss Mode 4 outside the working band. For instance, shortening the length of the strip and the side slot with slight modifications of other parameters. As shown in Fig. 16(b), the ECC of the $2 \times 2$ MIMO system is lower than 0.05 in the entire band, indicating remarkable MIMO performance. It can be known that the simulated results coincide well with that of the measurement. The deviation between the simulation and measurement is attributed to the fabrication tolerance, assembly error, and measurement error. Additionally, the proposed antenna is compatible with IFAs at the hinge slot and cavity antennas at the ground side, because the energy hardly propagates to the hinge slot and the cavity mode cannot be excite by the ground current.

The comparison among the proposed work and other works is presented in Table II. The type of IBW is marked at the upper right of the IBW data. It can be seen that though the sizes of the antennas in [5] and [11] are small, they do not fit for all-metal ID, and their LB efficiencies are low. The antennas in [21] and [22] are suitable for all-metal ID but have larger sizes, lower efficiencies, and narrower bandwidths. The designs in [23], [24], and [25] fit for all-metal ID and feature wide −6 dB IBWs and relatively high efficiencies.

TABLE II
COMPARISON AMONG THE PROPOSED WORK AND OTHER WORKS

| Ref. | IBW (%) LB/HB | Eff. (%) LB/HB | Antenna Size ($\lambda_{low}^2$) (1) | Clearance Area (mm$^2$) | Iso. (3) (dB) LB/HB |
|---|---|---|---|---|---|
| [5] | 6.4/19.5 $^{-10\text{dB}}$ | ≥51 / ≥82 | 0.07×0.043 | N.A. (2) | N.A. (4) |
| [11] | 3.5/42 $^{-10\text{dB}}$ | ≥40 / ≥61 | 0.178×0.028 | N.A. (2) | N.A. (4) |
| [21] | 4.5/36.8 $^{-6\text{dB}}$ | ≥38 / ≥60 | 0.24×0.08 | 10×30 | N.A. (4) |
| [22] | 7 $^{-6\text{dB}}$ | ≥10 | 0.35×0.052 | 8×40 | N.A. (4) |
| [23] | 28.7/44.5 $^{-6\text{dB}}$ | ≥65 / ≥55 | 0.058×0.012 | 10×180 | N.A. (4) |
| [24] | 10.6/32.9 $^{-10\text{dB}}$ | ≥64 / ≥82 | 0.352×0.016 | 2×44 | 10/15 |
| [25] | 47.6/54.8 $^{-6\text{dB}}$ | ≥51 / ≥51 | 0.14×0.014 | 8×290 | 17/15 |
| This work | 12.9/41.5 $^{-10\text{dB}}$ | ≥79 / ≥66 | 0.235×0.038 | 4.7×29.4 | 36/33 |

(1) $\lambda_{low}$ is the wavelength of the lowest frequency in the working band.
(2) Clearance area does not apply to non-all-metal ID laptops.
(3) Iso.: Isolation between MIMO elements.
(4) N.A.: The antennas are not MIMO antennas.

However, the −10 dB IBWs of [23] and [25] are narrower due to frequency mismatch. Due to the similar sizes of the laptops, clearance area is a physical dimension with a unit of "mm$^2$." The antennas in the first five references are not MIMO antenna, so the channel capacities of them are limited. Though the antenna system in [24] and [25] are MIMO systems, its isolation is lower than the proposed work owing to the small distance between the elements. Because the resonant modes of the long hinge slots are excited, the hinge slots in [23] and [25] must be considered in the clearance area, resulting in larger overall footprints than the proposed work. Despite the slightly smaller clearance area of the antenna in [24], its bandwidth is narrower. Moreover, the feeder of the antenna in [24], protruding from the metal cover, compromises the compatibility of all-metal ID and the reliability. The metal part feeder disconnected with two grounds and embedded in the protruding dielectric board decreases the structural integrity of the metal cover. The small gap (0.3 mm) between it and the screen ground makes the design relatively sensitive to small variations. In contrast, the proposed work is well compatible with all metal ID, and provides a stabler performance. In summary, the proposed antenna achieves a significantly small clearance area while offering superior dual-band and wideband performance, high efficiency, stable performance, and high isolation, providing a high concealment and compatibility with all-metal ID.

## V. CONCLUSION

In this communication, a dual-band Wi-Fi 6E antenna optimized for all-metal ID laptops is proposed. By integrating a folded $\pi$-shaped strip into the hinge-side slot, the antenna excites side-edge ground-plane currents, achieving broadband and high-efficiency radiation with an ultra-small clearance of $4.7 \times 29.4$ mm$^2$. The lower band radiation benefits from an extended effective aperture due to traveling-wave currents along the ground edge, while the high-frequency radiation originates from the slot opening, resembling a Vivaldi antenna. The $2 \times 2$ MIMO system, formed by placing two antennas in the hinge-side slots, achieves −10 dB impedance bandwidths of 2.29–2.48 GHz and 4.94–7.5 GHz, covering all Wi-Fi 6E bands (2.4G/5G/6G). It maintains high efficiency (>79% in LB, >66% in HB), low mutual coupling (< −33 dB), and an ECC below 0.03. This approach circumvents the limitations of traditional laptop antennas, ensuring seamless integration with all-metal enclosures without structural compromises.

## REFERENCES


[1] T.-W. Kang, K.-L. Wong, L.-C. Chou, and M.-R. Hsu, "Coupled-fed shorted monopole with a radiating feed structure for eight-band LTE/WWAN operation in the laptop computer," *IEEE Trans. Antennas Propag.*, vol. 59, no. 2, pp. 674–679, Feb. 2011.

[2] M. I. Magray, S. Su, and J. Lu, "Compact, hybrid slot-dipole-monopole Wi-Fi 7 antenna for slim-bezel notebook applications," in *Proc. Asia–Pacific Microw. Conf.*, Dec. 2023, pp. 28–30.

[3] H.-Y. Chien, C.-Y.-D. Sim, and C.-H. Lee, "Dual-band meander monopole antenna for WLAN operation in laptop computer," *IEEE Antennas Wireless Propag. Lett.*, vol. 12, pp. 694–697, 2013.

[4] Y. Liu, Y. Wang, and Z. Du, "A broadband dual-antenna system operating at the WLAN/WiMax bands for laptop computers," *IEEE Antennas Wireless Propag. Lett.*, vol. 14, pp. 1060–1063, 2015.

[5] B. Mun, C. Jung, M.-J. Park, and B. Lee, "A compact frequency-reconfigurable multiband LTE MIMO antenna for laptop applications," *IEEE Antennas Wireless Propag. Lett.*, vol. 13, pp. 1389–1392, 2014.

[6] I. F. Chen, C.-M. Peng, S.-M. Shen, D.-B. Lin, and K.-Y. Lee, "Bowtie-feed broadband monopole antenna for laptop applications," *IEEE Antennas Wireless Propag. Lett.*, vol. 10, pp. 1302–1304, 2011.

[7] C.-Y.-D. Sim, J. Kulkarni, S.-H. Wang, S.-Y. Zheng, Z.-H. Lin, and S.-C. Chen, "Low-profile laptop antenna design for Wi-Fi 6E band," *IEEE Antennas Wireless Propag. Lett.*, vol. 22, no. 1, pp. 79–83, Jan. 2023.

[8] Y. Zhang and Y. Li, "Wideband microstrip antenna in small volume without using fundamental mode," *Electromagn. Sci.*, vol. 1, no. 2, pp. 1–6, Jun. 2023.

[9] J.-H. Yang and H.-L. Su, "A broadband MIMO antenna array for WiFi-6E/7 in laptop computer applications," in *Proc. IEEE Int. Workshop Electromagnetics: Appl. Student Innov. Competition (iWEM)*, Jul. 2024, pp. 1–2.

[10] C.-Y.-D. Sim, W.-X. Zhu, C.-H. Chien, C.-H. Yiu, H.-D. Chen, and H.-M. Chen, "The design of a simple folded IFA for Wi-Fi 7 laptop applications," in *Proc. IEEE Int. Symp. Antennas Propag. INC/USNC-URSI Radio Sci. Meeting (AP-S/INC-USNC-URSI)*, Jul. 2024, pp. 775–776.

[11] C.-Y.-D. Sim, C.-C. Chen, X. Y. Zhang, Y.-L. Lee, and C.-Y. Chiang, "Very small-size uniplanar printed monopole antenna for dual-band WLAN laptop computer applications," *IEEE Trans. Antennas Propag.*, vol. 65, no. 6, pp. 2916–2922, Jun. 2017.

[12] H.-W. Liu, S.-Y. Lin, and C.-F. Yang, "Compact inverted-F antenna with meander shorting strip for laptop computer WLAN applications," *IEEE Antennas Wireless Propag. Lett.*, vol. 10, pp. 540–543, 2011.

[13] H. Li, Z. Zhou, Y. Zhao, and Y. Li, "Low-loss beam synthesizing network based on epsilon-near-zero (ENZ) medium for on-chip antenna array," *Chip*, vol. 2, no. 2, Jun. 2023, Art. no. 100049.

[14] Y. Zhang, Y. Li, W. Zhang, Z. Zhang, and Z. Feng, "Omnidirectional antenna diversity system for high-speed onboard communication," *Engineering*, vol. 11, pp. 72–79, Apr. 2022.

[15] K.-L. Wong and C.-Y. Tsai, "Half-loop frame antenna for the LTE metal-casing tablet device," *IEEE Trans. Antennas Propag.*, vol. 65, no. 1, pp. 71–81, Jan. 2017.

[16] K.-L. Wong and C.-Y. Huang, "Triple-wideband open-slot antenna for the LTE metal-framed tablet device," *IEEE Trans. Antennas Propag.*, vol. 63, no. 12, pp. 5966–5971, Dec. 2015.

[17] C.-K. Hsu and S.-J. Chung, "Compact antenna with U-shaped open-end slot structure for multi-band handset applications," *IEEE Trans. Antennas Propag.*, vol. 62, no. 2, pp. 929–932, Feb. 2014.

[18] H.-D. Chen, H.-W. Yang, and C.-Y.-D. Sim, "Single open-slot antenna for LTE/WWAN smartphone application," *IEEE Trans. Antennas Propag.*, vol. 65, no. 8, pp. 4278–4282, Aug. 2017.

[19] K.-L. Wong and Y.-C. Chen, "Small-size hybrid loop/open-slot antenna for the LTE smartphone," *IEEE Trans. Antennas Propag.*, vol. 63, no. 12, pp. 5837–5841, Dec. 2015.

[20] X. Li and Y. Wang, "A triple-port, triple-band Wi-Fi antenna covering the 2.4/5/6 GHz bands with a small clearance and high isolation for metal-bezel smartphones," *IEEE Antennas Wireless Propag. Lett.*, vol. 23, pp. 1814–1818, 2024.

[21] P.-H. Juan and S.-W. Su, "EMC hybrid loop/monopole LDS antenna with three-sided ground walls for 2.4/5/6 GHz WLAN operation," *IEEE Antennas Wireless Propag. Lett.*, vol. 22, pp. 2200–2204, 2023.

[22] Y. Li, Z. Zhang, Z. Li, J. Zheng, and Z. Feng, "High-permittivity substrate multiresonant antenna inside metallic cover of laptop computer," *IEEE Antennas Wireless Propag. Lett.*, vol. 10, pp. 1092–1095, 2011.

[23] S.-C. Chen and Y.-C. Tsou, "Small-size LTE/WWAN two-strip monopole exciter antenna integration with metal covers," *IEEE Trans. Antennas Propag.*, vol. 64, no. 8, pp. 3707–3711, Aug. 2016.

[24] S.-H. Cheng, S.-C. Chen, Y.-J. Chen, and C.-L. Liu, "Compact asymmetric T-Feed closed-slot antennas for 2.4/5/6 GHz WiFi-7 MIMO laptops," *Electronics*, vol. 13, no. 13, p. 2430, Jun. 2024.

[25] S.-C. Chen, P.-W. Wu, C. G. Hsu, and J.-Y. Sze, "Integrated MIMO slot antenna on laptop computer for eight-band LTE/WWAN operation," *IEEE Trans. Antennas Propag.*, vol. 66, no. 1, pp. 105–114, Jan. 2018.

[26] D. Schaubert, E. Kollberg, T. Korzeniowski, T. Thungren, J. Johansson, and K. Yngvesson, "Endfire tapered slot antennas on dielectric substrates," *IEEE Trans. Antennas Propag.*, vol. AP-33, no. 12, pp. 1392–1400, Dec. 1985.